Hindawi
Shock and Vibration
Volume 2020, Article ID 9041686, 15 pages
https://doi.org/10.1155/2020/9041686

Research Article

Experimental Study of Pressure Pulsation in a Mixed-Flow Pump with Different Tip Clearances Based on Wavelet Analysis

Leilei Ji,[1] Wei Li,[1,2] Weidong Shi,[3] Ling Zhou,[1] and Ramesh Agarwal[4]

[1]*Research Center of Fluid Machinery Engineering and Technology, Jiangsu University, Zhenjiang 212013, China*
[2]*Institute of Fluid Engineering Equipment Technology, Jiangsu University, Zhenjiang 212009, China*
[3]*College of Mechanical Engineering, Nantong University, Nantong 226019, China*
[4]*Department of Mechanical Engineering & Materials Science, Washington University in St. Louis, St. Louis, MO 63130, USA*

Correspondence should be addressed to Wei Li; lwjiangda@ujs.edu.cn and Weidong Shi; wdshi@ujs.edu.cn

Received 23 January 2020; Revised 28 April 2020; Accepted 1 July 2020; Published 25 July 2020

Academic Editor: Shuaishuai Sun

In order to investigate the effect of various impeller tip clearances on the pressure pulsation in a mixed-flow pump, the energy performance test and pressure pulsation experiment of a mixed-flow pump with different tip clearances are studied simultaneously. The pressure pulsation signals at impeller inlet, middle, and oulet are processed and analyzed by the wavelet transform. The results show that the change of tip clearance can affect the head and efficiency of mixed-flow pump. Under designed flow rate, when the tip clearance increases from 0.2 mm to 1.1 mm, the head and efficiency decrease by 18.1% and 11.6%, respectively. Due to the strong influence of blade passing frequency (BPF) at impeller middle, the period of pressure pulsation curve is about 1/4 of impeller rotation period. At impeller inlet, the low-frequency pulsation with energy concentration is the main disturbance frequency, and, with the increase of tip clearance, not only does the high-value region of wavelet spectrum expand to low-frequency direction but also it is easy to form second-order peaks in the time-averaged wavelet curve. At impeller outlet, affected by BPF and rotor-stator interaction (RSI), the high-frequency disturbance in RSI area decreases first and then increases. The wavelet coherence demonstrates the stable low-frequency disturbances in comparison to others and it will affect the flow field at impeller middle.

1. Introduction

The mixed-flow pump is a common hydrodynamic rotating mechanical device widely used in engineering [1–5] due to its moderate head and the capacity of transporting a larger flow rate. As the semiopen impeller is usually used in the mixed-flow pump, the internal flow fields of a mixed-flow pump are extremely complex and totally turbulent, including tip leakage flow (TLF) [6, 7], back flow [8], and vortex shedding from the blade tip region [9], as well as the RSI between the impeller and guide vane [10]. Among the all complex flows, the TLF, driven by the high-pressure gradient between the blade pressure surface and suction surface, will affect most of the flow fields of impeller flow channels and make the pump efficiency drop a lot [11]. The TLF will entrain with mainstream in impeller channel and form three types of vortexes: tip leakage vortex, tip separation vortex, and the induced vortex. Among the three types, the TLV occupies the dominant position. There is a sharp drop of pressure in the formation region of the TLV, which may lead to serious pressure pulsation and threaten the operation safety. Furthermore, the pressure pulsation in the mixed-flow pump is relatively strong enough to induce vibration of pump system and extra hydraulic forces together with some high-frequency noise [12, 13]. In fact, in the hydraulic design of mixed-flow pump [14], there is no relevant theory to support the design of tip clearance sizes, but the tip clearance size has a strong business with the strength of TLF. Therefore, it is necessary to do some researches of pressure pulsation of mixed-flow pump with different tip clearances to reveal the mechanism of TLF.

Up till now, with the rapid development of computational fluid mechanics (CFD) [15–20], many researches about the pressure pulsation and TLF have been carried out simultaneously, but those kinds of literature mostly focus on the flow structure of TLF and tip leakage vortex and there are few reports about the relationship between TLF and pressure pulsation. For instance, Liu et al. [21–23] conducted numerical simulations for a mixed-flow pump with different tip clearances using a commercial CFD code to study the tip leakage vortex structure and trajectory. They found that tip size slightly shifts the separation point of the primary tip leakage vortex but rarely affects the separation angle. Zhang et al. [24, 25] also numerically found the same feature that the starting point of tip leakage vortex that occurs near the impeller blade leading edge moves from leading edge to about 30% chord length at the design flow rate. Lei et al. [26] calculated the influence of T-shape tip clearance on performance of a mixed-flow pump and found that the leakage flow with T-shape blade end decreases by 15.95% compared with original blade end. Besides, pressure pulsation has been extensively investigated in mixed-flow pumps for several years, including pressure pulsation generated by inlet swirling flow [27] and RSI [28–30]. Miyabe et al. [31] used Dynamic Particle Image Velocimetry (PIV) and pressure pulsation measurements to investigate the propagation mechanism of a rotating stall. They found that the flow instabilities appear at 65% flow rate of BEP (Best Efficiency Point) because of a rotating stall. It was also found that unstable performance was caused by periodical large-scale abrupt backflow generated from the vaned diffuser to the outlet of impeller. Desheng et al. [32] numerically investigated the influence of blades and blade thickness on pressure pulsation of a mixed-flow pump in time domain. The results show that the pressure pulsation amplitudes in the inlet and outlet to the impeller are consistently increased when the number of impeller blades is reduced. Tan et al. [23, 33] investigated the role of blade rotational angle in the energy performance and pressure pulsation of a mixed-flow pump through an experimental measurement and numerical simulation. Also, they revealed the flow patterns of a mixed-flow pump with different tip clearance sizes by simulation. Wei et al. [34] found that the variation of tip clearance mainly affects the amount of leakage at impeller outlet by the pressure pulsation test of a pump with an oblique impeller near stall condition; and, with the increase of tip clearance, the radial velocity and axial velocity in the inlet flow field gradually increase from blade root to blade rim. Li et al. [35] also found that the tip clearance has a significant influence on the radial distribution of inlet pressure pulsation of mixed-flow pump impeller. As the tip clearance increases, the head of mixed-flow pump gradually decreases. However, most of these kinds of literature are conducted by CFD method, and the responses of high frequency in mixed-flow pumps could not be presented because of the limitation of computational source. Therefore, the experiments are used by some scholars to measure the pressure pulsation of mixed-flow pump [36–38]. However, the content of those literatures mostly introduced the pressure pulsation of fixed tip clearance. Thus, the understanding on generation mechanism and transportation characteristics of pressure pulsation of different tip clearances is still not satisfying. In particular, the influence of various tip clearances on pressure pulsation needs to be examined in detail. Therefore, to better understand the internal mechanism of various TLF, the pressure pulsation experiment is a practical method to reveal those characteristics. Unfortunately, so far, there are few literature studies about the experimental investigation of pressure pulsation in a mixed-flow pump with different tip clearances.

In this study, the experimental measurements of pressure pulsation in a mixed-flow pump with four tip clearances are conducted to reveal the influence of tip clearances, including the TLF, inlet flow fields, and the RSI between the impeller and guide vane. Firstly, the time domain of mixed-flow pump with different tip clearances is studied, and then the wavelet analysis is employed to investigate the pressure pulsation signals, which is more accurate to quantify the pressure pulsation than the method of fast Fourier transform (FFT) of unsteady pressure. In addition, the influence of blade tip clearance on pressure pulsation has been examined. The results could provide some references for improving the design of impeller and efficiency of mixed-flow pump.

2. Research Model

The objective research model is a low specific speed mixed-flow pump with guide vane. Figure 1 shows the geometry structure of the pump under investigation. Parameters of model pump are illustrated in Table 1. The parameters of mixed-flow pump investigated in this paper are as follows: the design flow rate $Q_{des} = 380\ m^3/h$, head $H = 6$ m, rotating speed $n = 1450$ r/min, number of blades $Z = 4$, and number of guide vanes $Z_d = 7$. Specific speed n_s is defined in the following equation:

$$n_s = \frac{3.65 \times n \times \sqrt{Q_{des}}}{H^{3/4}}, \tag{1}$$

where the units of all variables are consistent with those in Table 1. Therefore, $n_s = 480$. Pump inlet section diameter $D_{in} = 200$ mm, and outlet section diameter $D_{out} = 250$ mm. In order to install the model pump into test bed, the conical transition pipe is designed at the pump inlet for the connection. During test, the working medium is water at the temperature of 25°C. According to the recommended tip clearance size in [39], the optimum tip clearance is always 0.5% times the blade chord length. Thus, when the tip clearance is about 0.5 mm in this study, it is closest to the recommended size. In fact, up till now, there is still a debate on the selection of tip clearance size in mixed-flow pump, so three other kinds of tip clearance size (0.2 mm, 0.8 mm, and 1.1 mm) are chosen for analysis in this work.

3. Experimental Methods

3.1. Experimental Apparatus. The experimental measurements are conducted using Φ250 mm stainless steel closed test rig for mixed-flow pump in Research Center of Fluid Machinery Engineering and Technology, Jiangsu University.

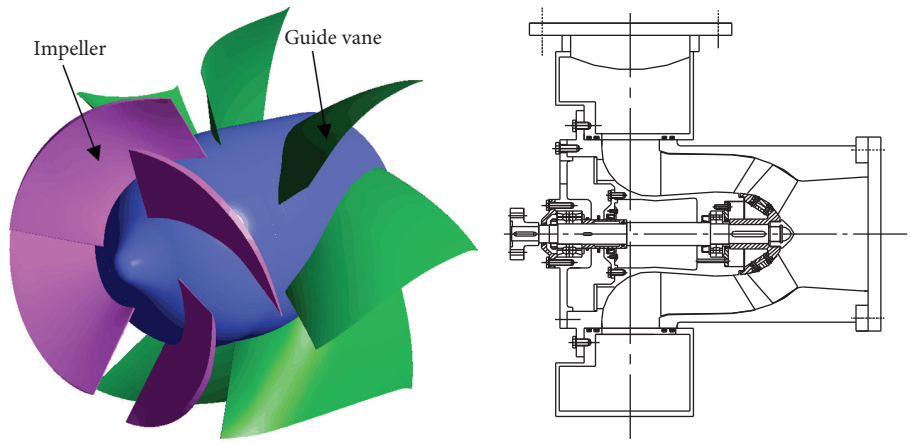

Figure 1: Mixed-flow pump model.

Table 1: Parameters of the mixed-flow pump model.

Parameters	Value
Design operating point	
Designed flow rate Q_{des} (m^3/h)	380
Designed rated head H (m)	6
Rated speed n (r/min)	1450
Specific speed n_s	480
Impeller	
Number of impeller blades Z	4
Width of the impeller b_2 (mm)	67.2
Inlet diameter of the impeller D_1 (mm)	185.2
Outlet diameter of the impeller D_2 (mm)	243.2
Average inlet blade angle β_1 (°)	24.9
Average outlet blade angle β_2 (°)	31.8
Tip clearance of blade t (mm)	0.2 mm, 0.5 mm, 0.8 mm, and 1.1 mm
Diffuser	
Number of guide vane blades Z_d	7
Inlet diameter D_3 (mm)	266.6
Outlet diameter D_4 (mm)	281.8
Average inlet blade angle α_3 (°)	45.6
Average outlet blade angle α_4 (°)	86.5
Pipe system	
Inlet diameter of the impeller D_{in} (mm)	200
Outlet diameter of the impeller D_{out} (mm)	250

The test bench meets the accuracy requirement of first class, and the experiment equipment is shown in Figure 2. The test rig mainly composed of a control valve, turbine flowmeter, regulator tank, cut-off valve, torque tachometer, model pump, and other components. The regulator tank is used to supply water and harmonize system pressure.

The energy performance parameters of the model pumps are measured by different devices. The torque tachometer (ZJ-type) with precision of 0.2 was used for the torque and the tachometric measurement. The turbine flowmeter (LWGY-type) with precision of 0.5 was set in the system to measure the flow rate. Besides, the pressure sensor (MPM-type) with 0.5% FS (full-scale) precision was equipped at the inlet and outlet of the mixed-flow pump to measure the pressure. Finally, the hydraulic machinery tester (HSJ-2010) was used to acquire experimental data from the above-mentioned sensors and all the signals were then transported from hydraulic machinery tester to the computer. The high-frequency pressure sensors are installed on the impeller end wall of different positions to measure the local pressure pulsation. The positions of the sensors are shown in Figure 3. The pressure pulsation of mixed-flow pump with different tip clearances ($t = 0.2$ mm, $t = 0.5$ mm, $t = 0.8$ mm, and $t = 1.1$ mm) under designed flow condition is collected. In order to ensure the implementation of different tip clearances, four impellers with different tip clearances are manufactured. During the implementation of impeller tip clearance, the feeler gauge is utilized to measure the size value of different positions along the blade chord to keep the tip clearance uniform. Three positions are selected to be measured during this test: the impeller inlet (A), middle (B), and outlet (C). Four pressure sensors are utilized and equally spaced 90° apart in the circumferential direction at each position. As all the sensors are installed on the pipe, the pressure signal obtained is the pressure pulsation near the wall. The output signal of pressure sensor ranges from 4 mA to 20 mA, and then the electric signal is converted to pressure signal by using a hydraulic machinery tester and computer.

3.2. Experimental Procedure. The external characteristic test and the pressure pulsation experiment are conducted simultaneously. All the following experimental procedures are applied to the experiment of mixed-flow pump with different kinds of tip clearance size. At the first procedure of experiment, all the experimental facilities are tested, and the supporting software of hydraulic machinery tester is debugged in order to record the pressure date successfully. The opening degree of the inlet valve and outlet valve are adjusted to the maximum at the beginning stage of the

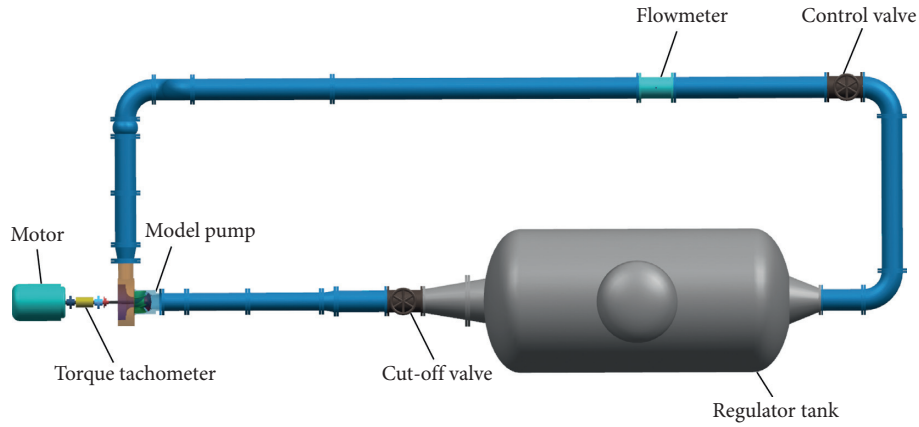

Figure 2: Experimental setup.

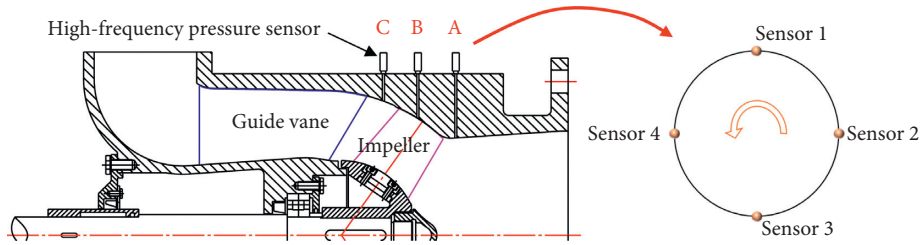

Figure 3: Mixed-flow pump model.

experiment as well. The converter power source has been turned on and the rotating speed of the pump is kept at 1450 r/min. The flow rate conditions are changed by adjusting the opening of the outlet valve. All the parameters of energy characteristics are recorded during the experiment. At the same time, the data of pressure pulsation experiment is also recorded. After finishing recording all the experimental data, the power source would be turned off. The above-mentioned experiment was repeated three times after the fluid in the test system became stable. The experimental site (left) and the installation location of the pressure sensor (right) are shown in Figure 4.

4. Results and Discussion

4.1. Comparison of Energy Performance under Different Tip Clearances. As can be seen from Figure 5, the energy performance of mixed-flow pump under four tip clearances is acquired. At the same tip clearance, as the flow rate increases, the head gradually decreases, and the efficiency value has a maximum value in the design conditions, indicating that the hydraulic pump has a better hydraulic design structure. Under different tip clearances, under the design flow conditions, when the tip clearance increases from 0.2 mm to 0.5 mm clearance, the changes in head and efficiency are not obvious. However, when the tip clearance increases from 0.5 mm to 1.1 mm, the head and efficiency decrease a lot obviously. Totally, when the tip clearance increases from 0.2 mm to 1.1 mm, although the tip clearance increased by 0.9 mm, the head and efficiency decreased by 18.1% and 11.6%, respectively. Under small flow conditions, the head change is more unstable under the flow rate condition of $0.4Q_{des}$. However, under large flow rate conditions, the changes of the head and efficiency under different tip clearance are not obvious. At the same time, from the smallest tip clearances to the largest tip clearance, the head and efficiency show an increasing trend first and then a decreasing trend. In summary, the tip clearance size has a great business with the energy performance of mixed-flow pump. When the tip clearance is 0.2 mm or 0.5 mm, the pump head or efficiency does not change much. However, when the tip clearance is 0.8 mm or 1.1 mm, the pump head or efficiency decreases significantly. These characteristics indicate that the tip clearance should be kept within 0.5 mm in this situation if the pump always operates under designed flow rate.

4.2. Time-Domain Characteristics of Pressure Coefficient under Different Tip Clearances. In this section, in order to study the effect of tip clearance size ($t = 0.2$ mm, $t = 0.5$ mm, $t = 0.8$ mm, and $t = 1.1$ mm) on the pressure pulsation of mixed-flow pump, the pressure pulsation distributions at the impeller inlet, impeller middle, and impeller outlet are acquired at designed flow rate. As transient relative pressure values at each monitoring point acquired by high-frequency pressure sensors are different according to the local position, the pressure pulsation coefficient is employed to normalize the relative pressure value. Meanwhile, the pressure pulsation coefficient is dimensionless and could eliminate the effect of flow rate conditions. Thus, the pressure pulsations of various positions could be compared with each other at

(a) (b)

Figure 4: Arrangement of external characteristic and pressure pulsation measurement.

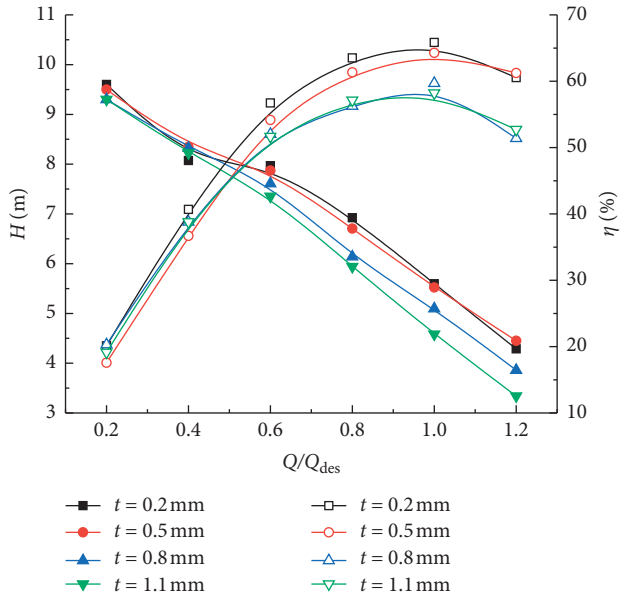

Figure 5: Comparison of energy performance curves with different tip clearances.

the same level. The pressure coefficient C_p could be expressed as

$$C_p = \frac{(1/N)\sum_{i=1}^{N}[P_i(t) - \overline{P}_i]}{0.5\rho u_2^2}, \quad (2)$$

where p is the relative static pressure measured by pressure sensor, Pa; u_2 is the circumferential velocity of impeller outlet, m/s; ρ is the density of water at room temperature, 1000 kg/m^3; N is the number of pressure pulsation signals.

Figure 6 shows the original time-domain characteristics of pressure pulsations of mixed-flow pump at the inlet, middle, and outlet of impeller at designed flow conditions with four tip clearances. For convenient analysis, a short segment of pressure signals is selected. It can be seen from the figure that the time-domain response of pressure pulsation at each monitoring point is rather large. At impeller inlet, the average amplitude of pressure pulsation in time-domain curve is smaller than that of other positions, and its periodicity is also weaker. At the middle of impeller, the periodicity of pressure coefficient pulsation curve is more obvious, and 4 peaks and troughs appeared within one impeller rotation cycle ($T = 0.0414$ s), which coincides with the BPF ($f \approx 96.68$ Hz). At the same time, the time-domain amplitude of pressure pulsation curve also increases significantly at the middle of impeller. At the impeller outlet, the average pressure pulsation amplitude reduces compared with the results of impeller middle, but the influence of BPF is still obvious. Specifically, the amplitude of pressure pulsation curve is still obvious, and the frequency of peaks and troughs is still large. Meanwhile, the RSI of impeller and guide vane is also obvious at the outlet of impeller. Four peak-to-peak differences in the pressure curve within a period are large, indicating that the unsteady effect of RSI zone is strong.

In terms of different tip clearances, the characteristics of pressure pulsation curve in each tip clearance are quite different at impeller inlet as well. When the tip clearance is smallest, the fluctuation intensity of time-domain curves varies greatly with time, and the maximum peak-to-peak difference of pressure pulsation curves in adjacent periods is about 0.1. With the increase of tip clearance, the peak-to-peak value of pressure coefficient curve decreases first and then increases. When the tip clearance is 0.5 mm, not only is the fluctuation amplitude of pressure curve low, but also the amplitude difference between the peak and trough value is not large. When the tip clearance is increased to 1.1 mm, the curve begins to show good periodicity and the fluctuation of pressure coefficient is relatively stable. At this time, the time of pressure curve elapsed in one cycle is about 0.06 s (as shown by red dashed line), which is slightly larger than the rotation period of impeller. At the middle of impeller, the difference in pressure pulsation curves of different tip clearances is not obvious, and the period of pressure pulsation curve is about 1/4 of impeller rotation period resulting from the influence of BPF. However, the periodicity of pressure pulsation curve of 0.5 mm tip clearance is better

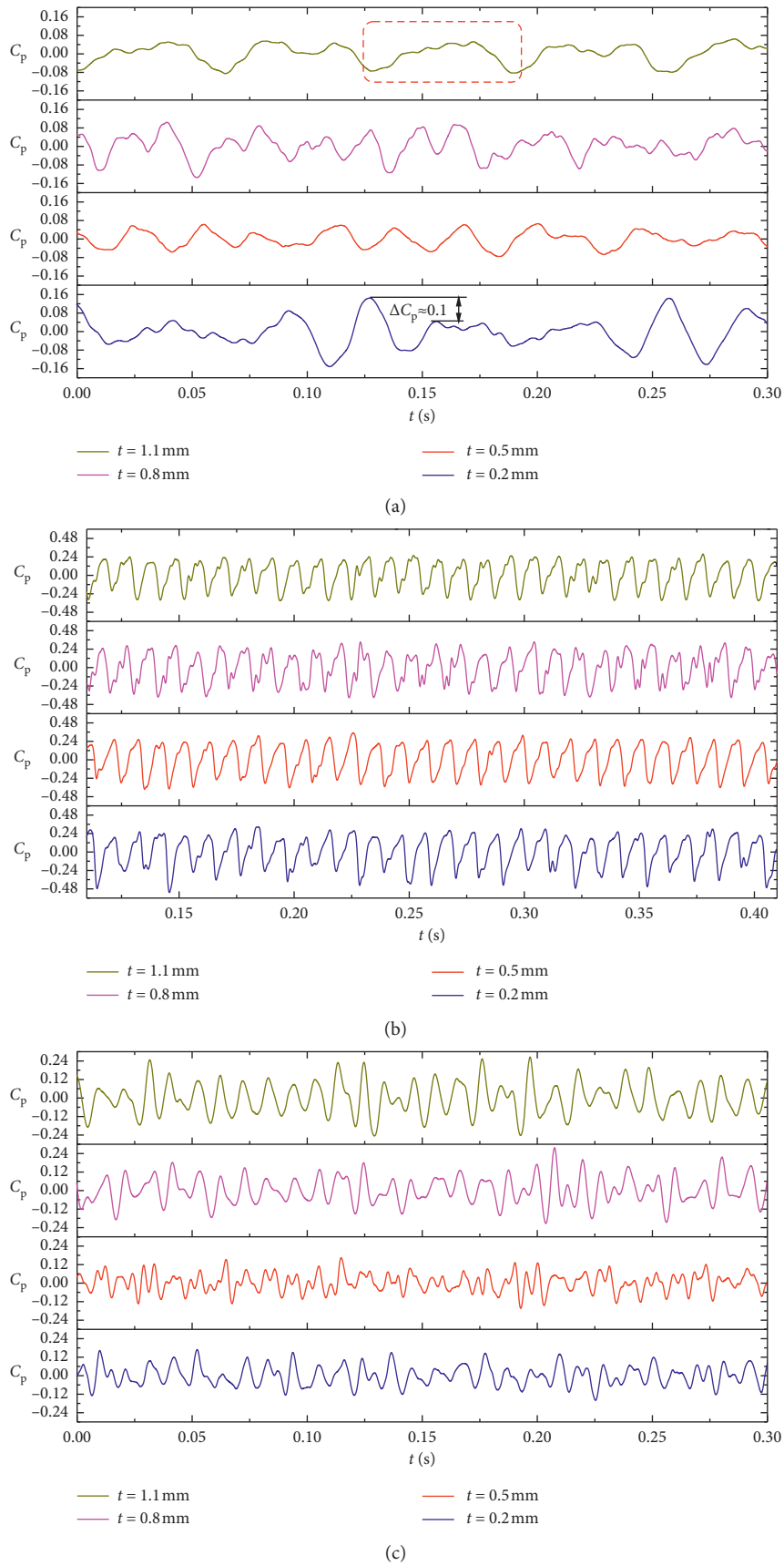

Figure 6: Time-domain characteristic of impeller inlet, middle, and outlet under different tip clearances. (a) Impeller inlet. (b) Impeller middle. (c) Impeller outlet.

than that of the other three tip clearances. There is a difference between the peak and trough value of pressure amplitude within different impeller rotation cycles when the tip clearance is small, while the harmonic components of pressure curve increase significantly when the large tip clearance is large. At impeller outlet, under the dual influence of BPF and RSI between impeller and guide vane, there is more information in the pressure coefficient curve of each tip clearance, which is not easy to be distinguished. In general, with the increase of tip clearance, the amplitude of pressure pulsation also shows a decreasing trend first and then an increasing trend. In summary, the size of tip clearance does affect the pressure pulsation characteristics of impeller inlet, middle, and outlet of mixed-flow pump, while the impeller inlet and impeller outlet are significantly more affected in comparison to impeller middle.

4.3. Wavelet Transform of Pressure Pulsation under Different Tip Clearances. It is known that the time-domain signals of pressure pulsation could only provide the characteristics with time, and the characteristics in frequency space could not be described. In recent years, the emergence of continuous wavelet transform can not only describe the change of signals with time but also obtain the characteristics of signals in spatial frequency. Therefore, continuous wavelet transform is used in this section to analyze pressure pulsation signals. The energy spectrum function of the continuous wavelet transform is defined as

$$W_X(s,t) = \int_{-\infty}^{+\infty} x(\tau)\psi^*\left(\frac{\tau - t}{s}\right)\mathrm{d}\tau, \tag{3}$$

where $x(\tau)$ is the time series signal; $W_X(s,\tau)$ is the wavelet transform coefficient; $\psi^*(\tau)$ is the conjugate function of wavelet function.

Unlike the Fourier transform whose basis is always orthogonal, the choice of wavelet base is more versatile. For the same time series, different wavelet bases can lead to a completely different spectrum. Therefore, the choice of wavelet base is crucial to wavelet analysis. In this study, the wavelet base function used is the derivative of a Gaussian (DOG), which is better for the application to tip flows.

The wavelet base function is as follows:

$$\begin{aligned}\psi_0(\tau) &= \frac{(-1)^{m+1}}{\sqrt{\Gamma(m+1/2)}}\frac{d^m}{\mathrm{d}t^m}\left(e^{-\tau^2/2}\right),\\ \widehat{\psi}_0(\omega) &= \frac{(-i)^{m+1}}{\sqrt{\Gamma(m+1/2)}}(s\omega)^m e^{-(s\omega)^2/2}.\end{aligned} \tag{4}$$

The wavelet base is normalized by

$$\int_{-\infty}^{\infty}\left|\widehat{\psi}_0(\omega')\right|^2\mathrm{d}\omega' = 1, \tag{5}$$

where m is the derivate order and ω is the frequency.

Figure 7 shows the wavelet transform results with wavelets of different frequency-space resolutions at the inlet, middle, and outlet of the impeller under different clearances. The times of pressure signals have been transferred to the number of revolutions of impeller, which could be abbreviated as Rev. The method to relate wavelet scale s to Fourier frequency can be found in [40]. In order to weaken the edge effects and error of finite length of experimental signals [41], the number of pressure pulsation signals, which is corresponding to the integer power of 2, has been selected to be analyzed. Also, the time-averaged wavelet spectrum is shown on the right side of each wavelet transform figure. It can be seen from the figure that most of the energy of wavelet spectrum is basically concentrated from 8 Hz to 64 Hz under different tip clearances, and the modulus value of the first-order peak formed in the time-averaged wavelet spectrum curve is higher. However, compared with other gaps, the frequency range of energy concentration is narrower when the tip clearance is 0.2 mm, nearly from 16 Hz to 64 Hz, which indicates that the pressure signal at impeller inlet under small tip clearance is more stable and periodic. With the increase of tip clearance, the high-energy value region of the wavelet spectrum expands towards the low frequency, and the second-order peak is formed when the tip clearance is 0.5 mm or 0.8 mm, and the second-order peak value at 0.8 mm is significantly higher than that of 0.5 mm. However, the time-averaged wavelet spectrum in the low-frequency band is significantly higher under the tip clearance of 0.5 mm, indicating that the low-frequency disturbance at impeller inlet is obvious currently. With the increase of tip clearances, the energy of wavelet spectrum changes greatly. For instance, when the tip clearance is 1.1 mm, the frequency corresponding to the first-order peak of wavelet spectrum significantly reduces, while the frequency corresponding to the second-order peak is higher, indicating that the main frequency pulsation of impeller inlet has changed at large tip clearances. At the same time, comparing the time-averaged wavelet spectra of four tip clearances, it is found that the extreme value of wavelet spectrum decreases rapidly and then increases slightly with the increase of tip clearance, and the extreme value tends to be stable at two large tip clearances. This shows that although the increase of TLF reduces the disturbance frequency at impeller inlet under large tip clearances, the intensity of the disturbance does not increase much.

Similarly, Figure 8 shows the wavelet modulus spectrum and time-averaged wavelet modulus spectrum curve at impeller middle with different tip clearances. Under the circumstance of different tip clearances, the first-order peaks of the wavelet spectrum stand from 64 Hz to 128 Hz, which is consistent with the frequency band where BPF is, indicating that the impeller middle of four tip clearances is significantly affected by the BPF. However, it can be seen from the time-averaged wavelet spectrum that as tip clearance increases, the time-averaged value of wavelet modulus spectrum gradually decreases, indicating the intensity of pressure pulsation caused by TLF from impeller blade middle rim decreases, further explaining that the pressure difference on both sides of blades at impeller middle reduces.

Figure 9 shows the wavelet modulus spectrum and time-averaged wavelet modulus spectrum curve at impeller outlet with different tip clearances. As can be seen from the figure, the energy distribution of wavelet spectrum at impeller

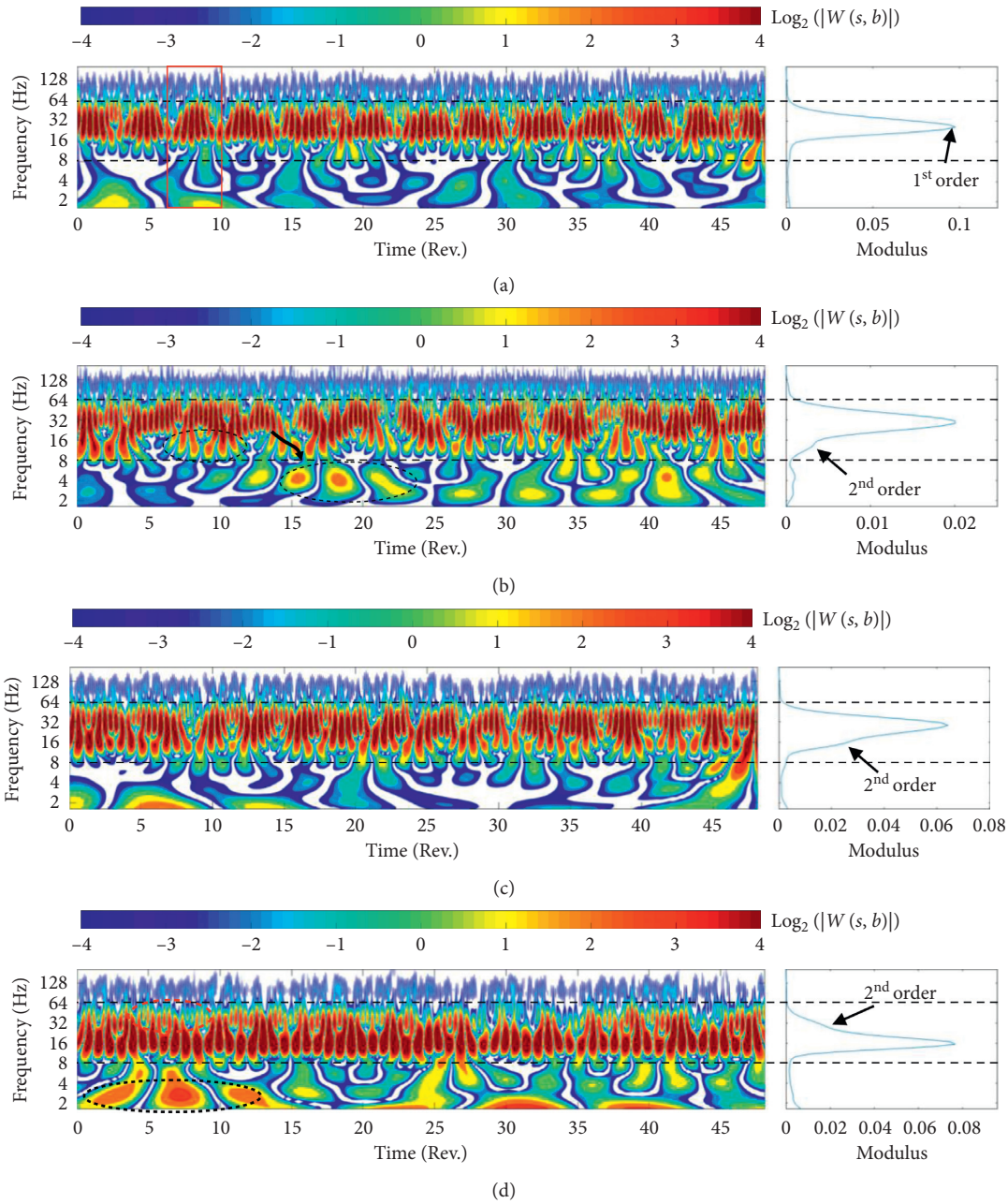

FIGURE 7: Wavelet modulus spectrum of pressure pulsation at impeller inlet with different tip clearances. (a) $t = 0.2$ mm. (b) $t = 0.5$ mm. (c) $t = 0.8$ mm. (d) $t = 1.1$ mm.

outlet is quite different under different tip clearances, so the wavelet spectrum is divided into high-frequency bands and low-frequency bands for analysis, which is marked with dashed lines. In general, compared with the four tip clearances, the wavelet energy is still concentrated in high-frequency band, indicating that the influence of BPF is still obvious. Among four tip clearances, the wavelet energy concentration in the high-frequency region is the best at 0.5 mm tip clearance, and most of the high-frequency energy is in the interval of 64–128 Hz. However, when the tip clearance decreases or increases, part of the energy in the high-frequency region overflows toward the high-frequency direction. That is, when the frequency is greater than 128 Hz, the wavelet energy spectrum value is still high. At the same time, it can be seen from the first-order peak value of the time-averaged wavelet spectrum that the extreme value of time-averaged wavelet energy also decreases first and then increases with the increase of tip clearance. Within low-frequency band, the value of wavelet energy spectrum is also higher under the situation of four tip clearances as a result of the RSI effect. At 0.5 mm tip clearance, the wavelet energy in the low-frequency band does not fluctuate much in

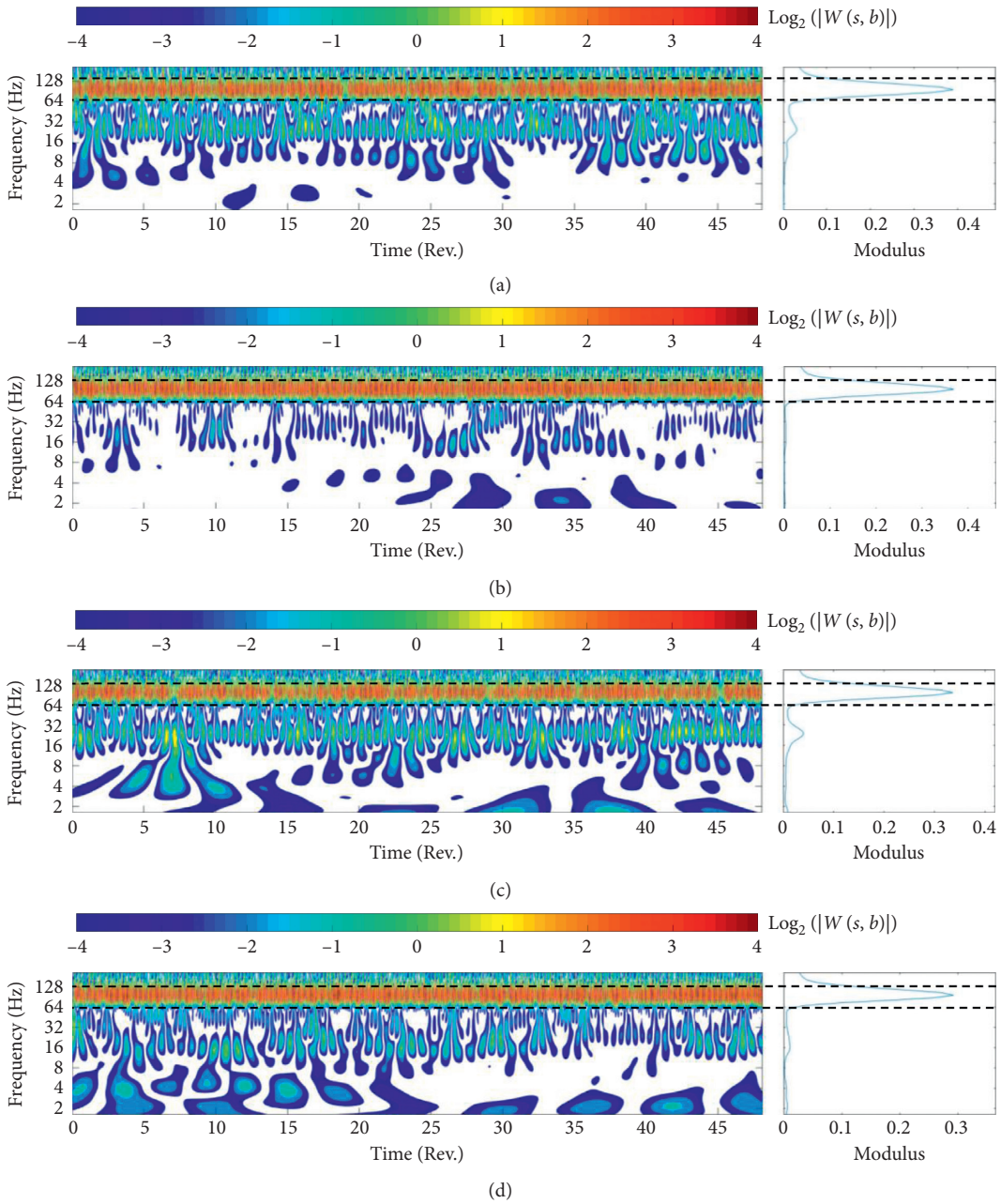

Figure 8: Wavelet modulus spectrum of pressure pulsation at impeller middle with different tip clearances. (a) $t = 0.2$ mm. (b) $t = 0.5$ mm. (c) $t = 0.8$ mm. (d) $t = 1.1$ mm.

frequency space, and the time-average wavelet modulus value is small. However, under the circumstance of other tip clearances, the time-averaged wavelet energy fluctuates greatly, and the second-order peaks are obvious. Like wavelet energy distribution within the high-frequency band, the wavelet energy extreme value decreases first and then increases within the low-frequency band as the tip clearance increases. These phenomena indicate that the size of tip clearance can indirectly affect the flow fields in the RSI zone. As the tip clearance increases, the high-frequency disturbance in RSI zone decreases first and then increases, so there is an optimal tip clearance value of impeller in which the smallest disturbance exists.

4.4. Coherence of Pressure Pulsation under Different Tip Clearances. In mathematics, coherence refers to the content of correlation between two variables. The wavelet coherence analysis has a strong ability to analyze non-steady-state models in the process of pressure pulsation signals. For two time series pressure pulsation signals $x(t)$ and $y(t)$, the wavelet coherence spectrum between them can be defined as

$$R^2(a,b) = \frac{\left|S\left(a^{-1}W_{XY}(a,b)\right)\right|^2}{S\left(a^{-1}W_X(a,b)\right)S\left(a^{-1}W_Y(a,b)\right)}, \tag{6}$$

where $R(a,b)$ is coherence coefficient and S is smoothing operator.

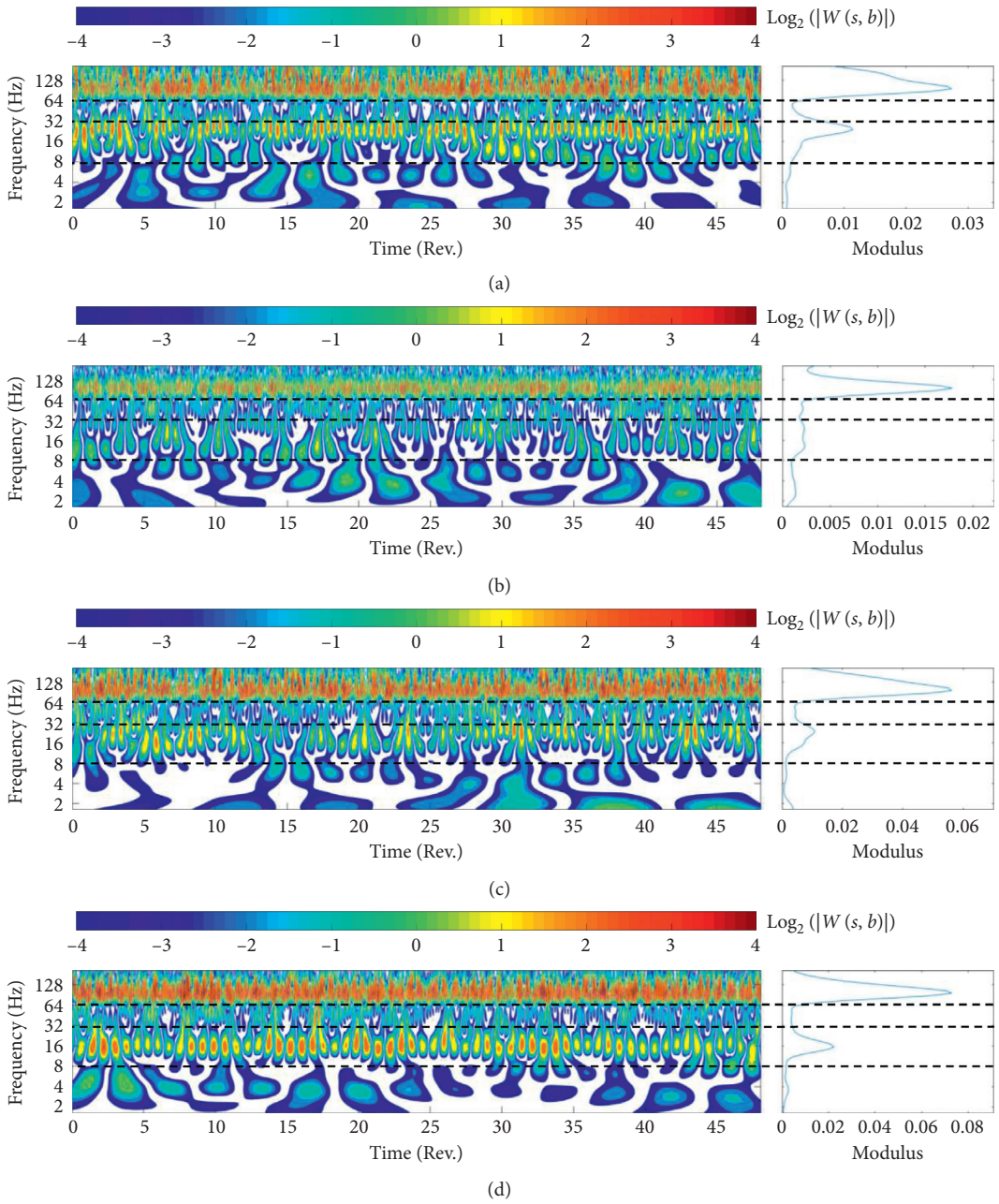

FIGURE 9: Wavelet modulus spectrum of pressure pulsation at impeller outlet with different tip clearances. (a) $t = 0.2$ mm. (b) $t = 0.5$ mm. (c) $t = 0.8$ mm. (d) $t = 1.1$ mm.

In order to further analyze the coherence of pressure signals at different locations, a wavelet transform coherence (WTC) analysis is performed on the dynamic pressure pulsation signals collected under the tip clearance of 0.5 mm. In the analysis process, adjacent pressure sensors (sensor 1 and sensor 2) and axisymmetrical pressure sensors (sensor 1 and sensor 3) are selected for coherence analysis processing, respectively. Figures 10 and 11 are the wavelet coherence spectrum obtained from adjacent pressure sensors and axisymmetrical pressure sensors in the same axial section when the tip clearance is 0.5 mm, respectively. On the right side of wavelet coherence spectrum, time-averaged results of wavelet coherence spectrum are shown simultaneously, as shown in the previous sections. For more convenience of analysis, the signals of different positions are divided into three kinds. The first is from 2 Hz to 16 Hz, which is named L-region. The second is from 16 Hz to 64 Hz, which is named M-region. The third is from 64 Hz to maximum, which is named H-region. Because of the signal edge effect, the error is higher in the COI (cone of influence) region; only the wavelet coherence in the confidence interval is studied. It can be seen from the figure that, no matter whether the distance of two sensors is far or close, the wavelet coherence is strong near the BPF and within 2~16 Hz at the section of

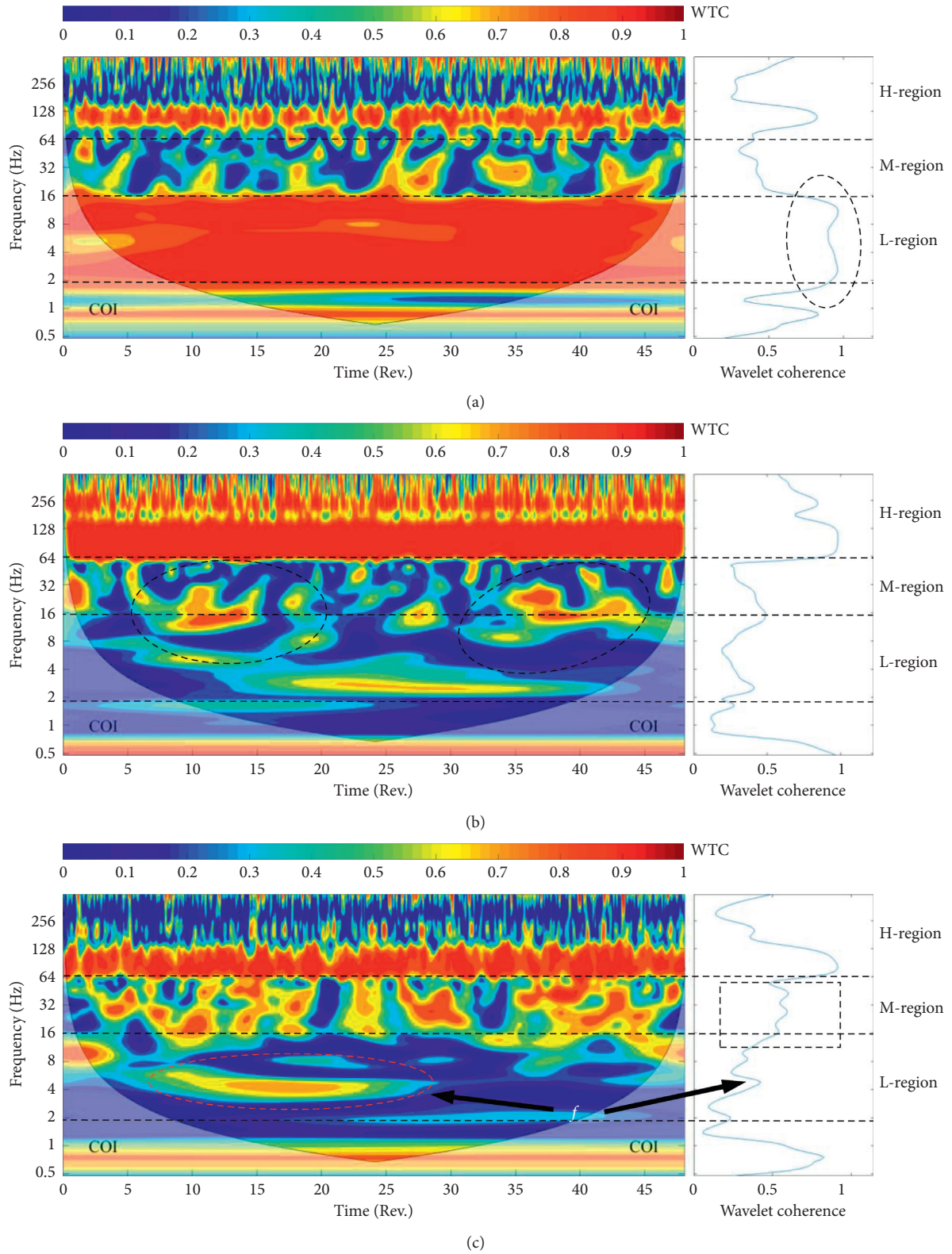

Figure 10: Wavelet coherence spectrum of pressure pulsation of adjacent pressure sensors with different tip clearances. (a) Impeller inlet. (b) Impeller middle. (c) Impeller outlet.

impeller inlet. It indicates that the similarity of two time series pressure signals is high in frequency spaces. Furthermore, the wavelet coherence of pressure pulsation becomes lower when two pressure sensors distribute asymmetrically, but it still shows the high coherence region, which indicates that the inlet disturbance is stable at the

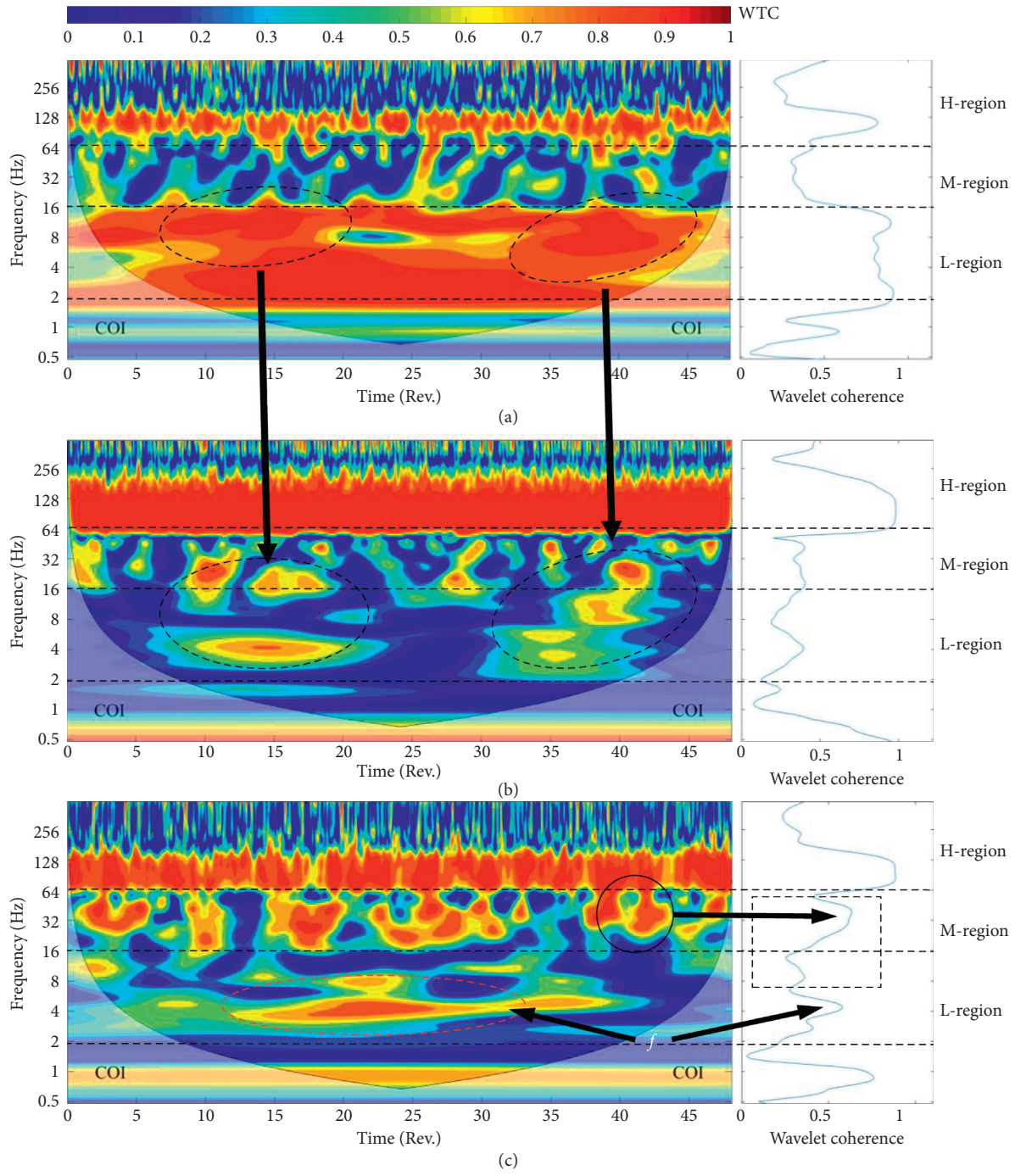

Figure 11: Wavelet coherence spectrum of pressure pulsation of axisymmetrical pressure sensors with different tip clearances. (a) Impeller inlet. (b) Impeller middle. (c) Impeller outlet.

impeller inlet. At the same time, it can be known that the flow field at the impeller inlet is mainly affected by the disturbance of low frequency and BPF, which is consistent with the analysis of the wavelet spectrum. However, the wavelet coherence spectrum shows that the low-frequency fluid disturbance is relatively stable in different positions, and the influence of BPF on impeller inlet is unstable.

At impeller middle, there is not much difference between the two sets of wavelet coherence spectrum, both of which have high coherence between 64 Hz and 128 Hz, indicating that the two sets of signals are affected by the stable BPF and also the stability of impeller rotational speed. In the intermediate frequency region and low-frequency region, the wavelet coherence spectrum of two group shows weaker wavelet coherence, but strong coherence value appears only at some moments, such as in the interval of 10~15 Rev and 35~45 Rev. In fact, these two regions correspond to the high coherence in the low-frequency band of impeller inlet from

the coherence spectrum of axisymmetric sensors, which indicates that the low-frequency disturbance of impeller inlet will also affect the flow fields of impeller middle to a certain extent, but the impact is not great. At impeller outlet, the wavelet coherence value near BPF is still high, and the intensity of wavelet coherence shows a decreasing trend as the frequency drops in the intermediate-frequency space and low-frequency space. Comparing the wavelet coherence spectrum of two pairs of pressure sensors, the time-averaged coherence difference at the intermediate frequency band is significantly different, followed by the low-frequency band. Within intermediate frequency band, when the sensors are adjacent, the interaction between adjacent flow channels makes the correlation signal between the pressure pulsation signals, so the coherence of the entire frequency band is strong. When two sensors are far away, there is an isolated flow channel between the corresponding flow channels, so the interaction effects reduce, and the coherence strength of the low-frequency region of the intermediate frequency band is weakened. However, at this time, the coherence in the high-frequency part of intermediate frequency band is still strong, and it is located near the axial frequency of impeller, indicating that the axial frequency disturbance is strong locally. Therefore, the distance between sensors is also one of the factors affecting coherence. In the low-frequency band, the coherence between the two sets of pressure pulsation signals is further weakened, but the coherence is also greater at some moments. When two sensors are close, the maximum coherence appears near 18 Rev, and when two sensors are far away, the maximum coherence appears near 22 Rev, indicating that the signal has a random pulsation and nonstationarity.

5. Conclusions

In this paper, the energy performance and pressure pulsation characteristics of a mixed-flow pump under different tip clearances are analyzed based on wavelet analysis; some findings are as follows:

(1) The change of tip clearance can affect the head and efficiency of mixed-flow pump. Under different clearances, when the tip clearance increases from 0.2 mm to 1.1 mm, the head and efficiency decreased by 18.1% and 11.6%, respectively, under designed flow rate condition. When the tip clearance is 0.2 mm or than 0.5 mm, the pump head or efficiency does not change much. However, when the tip clearance is 0.8 mm or than 1.1 mm, the pump head or efficiency decreases significantly. Therefore, in order to ensure that the mixed-flow pump operates at a higher head and efficiency point, the tip clearance of the impeller needs to be kept at a small level.

(2) The size of tip clearance of mixed-flow pump affects the time-domain characteristics of pressure pulsation. Due to the strong influence of BPF of four blades at the middle of impeller, the period of pressure pulsation curve is about 1/4 of impeller rotation period, and the effect of tip clearance change is not obvious compared with the impeller inlet and impeller outlet. The amplitude and intensity of pressure pulsation at impeller inlet are mainly affected by the change of tip clearances. With the increase of tip clearance, the peak-to-peak value of pressure pulsation curve and the fluctuation degree of pressure pulsation show a decreasing trend first and then an increasing trend. Meanwhile, the change of tip clearance also makes the time-domain features of impeller outlet more complicated.

(3) Compared with the similar wavelet spectrum of pressure pulsation at impeller middle, the pressure wavelet energy spectra at the impeller inlet and the impeller outlet are significantly different. At impeller inlet, the low-frequency pulsation with energy concentration is the main disturbance frequency, and, with the increase of tip clearance, not only does the high-value region of wavelet spectrum expand to low-frequency direction, but also it is easy to form second-order peaks in the time-averaged wavelet curve. Although the main frequency pulsation of impeller inlet under the large tip clearance reduces, the increase of disturbance intensity is not obvious. At impeller outlet, affected by BPF and RSI, the extreme value of the time-averaged wavelet curve also decreases first and then increases with the increase of tip clearance, indicating that the high-frequency disturbance in RSI area decreases first and then increases. Therefore, there is an optimal tip clearance value to make the minimum disturbance.

(4) The wavelet coherence at different positions indicates a higher similarity of low-frequency pulsation at impeller inlet in the circumferential direction, also demonstrating that the low-frequency disturbances of impeller inlet flow field are more stable than those in other positions, but the low-frequency disturbances in impeller inlet still affect the low-frequency pulsation at impeller middle. There is still a high degree of coherence at different positions of impeller outlet impacted by BPF, and the coherence at the intermediate frequency band is not weak as well. The interaction between adjacent flow channels also makes the coherence between adjacent pressure sensors in intermediate frequency band stronger, but when the two sensors are far away, the interaction between flow channels weakens. However, the coherence of axial frequency is strong, which indicates that the axial frequency disturbance is strong there. Therefore, sensor distance is also one of the most important factors for coherence analysis.

Data Availability

The data used to support the findings of this study are included within the article. Some of the authors' data processing code written by C. Torrence and G. Compo is available at https://paos.colorado.edu/research/wavelets/ and that by Grinsted et al. is available at http://www.glaciologynet/wavelet-coherence.

Conflicts of Interest

The authors declare that there are no conflicts of interest regarding the publication of this paper.

Acknowledgments

This work was sponsored by the National Natural Science Foundation of China (nos. 51679111 and 51409127), National Key R&D Program Project (no. 2017YFC0403703), PAPD, Six Talents Peak Project of Jiangsu Province (no. HYZB-002), Key R&D Program Project in Jiangsu Province (BE2016319 and BE2017126), Natural Science Foundation of Jiangsu Province (no. BK20161472), Science and Technology Support Program of Changzhou (no. CE20162004), Key R&D Program Project of Zhenjiang (no. SH2017049), Scientific Research Start Foundation Project of Jiangsu University (no. 13JDG105), Synergistic Innovation Center of Jiangsu Modern Agricultural Equipment and Technology (4091600014), and Graduate Research and Innovation Project of Jiangsu Province (SJKY19_2552). The first author would like to acknowledge Chinese Scholarship Council (CSC) for the financial support and Washington University in St. Louis for providing the opportunity to spend a year as a visiting Ph.D. student (201908320291).

References

[1] Z. Chen, W. Shi, D. Zhang, J. Zhang, and Z. Zhang, "Experimental study on cavitation characteristics of mixed-flow pump during startup," *Journal of Drainage and Irrigation Machinery Engineering*, vol. 37, no. 9, pp. 758–762, 2019.

[2] L. Zhang, W. Shi, D. Zhang, and L. Shi, "Analysis of instability flow on mixed-flow pump based on LES," *Journal of Drainage and Irrigation Machinery Engineering*, vol. 35, no. 4, pp. 303–308, 2017.

[3] L. Wei, P. Yuanfeng, W. Shi, L. Ji, E. Li, and L. Ma, "Research progress in rotating stall in mixed-flow pumps with guide vane," *Journal of Drainage and Irrigation Machinery Engineering*, vol. 37, no. 9, pp. 737–745, 2019.

[4] S. Yang, K. Shao, and T. DAI, "Influence of blade wrap angle on characteristics of mixed flow pump as turbine," *Journal of Drainage and Irrigation Machinery Engineering*, vol. 37, no. 6, pp. 475–479, 2019.

[5] L. Ji, W. Li, W. Shi, H. Chang, and Z. Yang, "Energy characteristics of mixed-flow pump under different tip clearances based on entropy production analysis," *Energy*, vol. 199, Article ID 117447, 2020.

[6] Z. Yu, W. Zhang, B. Zhu, and Y. Li, "Numerical analysis for the effect of tip clearance in a low specific speed mixed-flow pump," *Advances in Mechanical Engineering*, vol. 11, no. 3, 2019.

[7] W. Li, R. K. Agarwal, L. Zhou, E. Li, and L. Ji, "Effect of tip clearance on rotating stall in a mixed-flow pump," in *Proceedings of the ASME Turbo Expo 2019: Turbomachinery Technical Conference and Exposition*, American Society of Mechanical Engineers Digital Collection, Phoenix, AZ, USA, June 2019.

[8] W. Cao, W. Li, L. Ji, W. Shi, Z. Lu, and R. K. Agarwal, "Research of transient rotor–stator interaction effect in a mixed-flow pump under part-load conditions," *Journal of the Brazilian Society of Mechanical Sciences and Engineering*, vol. 42, no. 1, p. 36, 2020.

[9] Y. Liu and L. Tan, "Spatial–temporal evolution of tip leakage vortex in a mixed-flow pump with tip clearance," *Journal of Fluids Engineering*, vol. 141, no. 8, Article ID 081302, 2019.

[10] H. Wu, R. L. Miorini, and J. Katz, "Measurements of the tip leakage vortex structures and turbulence in the meridional plane of an axial water-jet pump," *Experiments in Fluids*, vol. 50, no. 4, pp. 989–1003, 2011.

[11] D. You, M. Wang, R. Mittal, and P. Moin, "Study of tip-clearance flow in turbomachines using large-eddy simulation," *Computing in Science & Engineering*, vol. 6, no. 6, p. 38, 2004.

[12] W. Li, L. Ji, W. Shi et al., "Correlation research of rotor–stator interaction and shafting vibration in a mixed-flow pump," *Journal of Low Frequency Noise, Vibration and Active Control*, vol. 39, no. 1, pp. 72–83, 2019.

[13] W. Li, L. Ji, W. Shi, Y. Wang, L. Zhou, and X. Jiang, "Vibration of shaft system in the mixed-flow pump induced by the rotor-stator interaction under partial load conditions," *Shock and Vibration*, vol. 2018, Article ID 2059784, 12 pages, 2018.

[14] Y. Gu, J. Pei, S. Yuan, and J. Zhang, "A pressure model for open rotor-stator cavities: an application to an adjustable-speed centrifugal pump with experimental validation," *Journal of Fluids Engineering*, vol. 142, no. 10, 2020.

[15] N. Zhang, X. Liu, B. Gao, X. Wang, and B. Xia, "Effects of modifying the blade trailing edge profile on unsteady pressure pulsations and flow structures in a centrifugal pump," *International Journal of Heat and Fluid Flow*, vol. 75, pp. 227–238, 2019.

[16] W. Zhou, N. Qiu, L. Wang, B. Gao, and D. Liu, "Dynamic analysis of a planar multi-stage centrifugal pump rotor system based on a novel coupled model," *Journal of Sound and Vibration*, vol. 434, pp. 237–260, 2018.

[17] N. Zhang, B. Gao, Z. Li, D. Ni, and Q. Jiang, "Unsteady flow structure and its evolution in a low specific speed centrifugal pump measured by PIV," *Experimental Thermal and Fluid Science*, vol. 97, pp. 133–144, 2018.

[18] P. Tang, H. Li, Z. Issaka, and C. Chen, "Effect of manifold layout and fertilizer solution concentration on fertilization and flushing times and uniformity of drip irrigation systems," *Agricultural Water Management*, vol. 200, pp. 71–79, 2018.

[19] Z. Issaka, H. Li, Y. Jiang, P. Tang, and C. Chao, "Comparison of rotation and water distribution uniformity using dispersion devices for impact and rotary sprinklers," *Irrigation and Drainage*, vol. 68, no. 5, pp. 881–892, 2019.

[20] H. Li, Z. Issaka, Y. Jiang, P. Tang, and C. Chen, "Influence of a fixed water dispersion device on jet dispersion and range from an impact sprinkler," *Irrigation and Drainage*, vol. 68, no. 4, pp. 669–678, 2019.

[21] Y. Liu and L. Tan, "Theoretical prediction model of tip leakage vortex in a mixed flow pump with tip clearance," *Journal of Fluids Engineering*, vol. 142, no. 2, 2020.

[22] Y. Liu and L. Tan, "Investigation of tip leakage vortex characteristics around tip clearance in a mixed flow pump," *IOP Conference Series: Earth and Environmental Science*, vol. 240, no. 3, Article ID 032014, 2019.

[23] Y. Liu, L. Tan, Y. Hao, and Y. Xu, "Energy performance and flow patterns of a mixed-flow pump with different tip clearance sizes," *Energies*, vol. 10, no. 2, p. 191, 2017.

[24] D. Zhang, D. Pan, Y. Xu, P. Shao, and G. Wang, "Numerical investigation of blade dynamic characteristics in an axial flow pump," *Thermal Science*, vol. 17, no. 5, pp. 1511–1514, 2013.

[25] D. Zhang, D. Pan, W. Shi, S. Wu, and P. Shao, "Study on tip leakage vortex in an axial flow pump based on modified shear stress transport k-ω turbulence model," *Thermal Science*, vol. 17, no. 5, pp. 1551–1555, 2013.

[26] T. Lei, X. Zhifeng, L. Yabin, H. Yue, and X. Yun, "Influence of T-shape tip clearance on performance of a mixed-flow pump," *Proceedings of the Institution of Mechanical Engineers, Part A: Journal of Power and Energy*, vol. 232, no. 4, pp. 386–396, 2018.

[27] L. Ji, W. Li, and W. Shi, "Influence of tip leakage flow and inlet distortion flow on a mixed-flow pump with different tip clearances within the stall condition," *Proceedings of the Institution of Mechanical Engineers, Part A: Journal of Power and Energy*, vol. 234, no. 4, pp. 433–453, 2019.

[28] W. Li, L. Zhou, W.-d. Shi, L. Ji, Y. Yang, and X. Zhao, "PIV experiment of the unsteady flow field in mixed-flow pump under part loading condition," *Experimental Thermal and Fluid Science*, vol. 83, pp. 191–199, 2017.

[29] C. Hao, S. Weidong, L. Wei et al., "Experimental optimization of jet self-priming centrifugal pump based on orthogonal design and grey-correlational method," *Journal of Thermal Science*, vol. 29, no. 1, pp. 241–250, 2020.

[30] L. Ji, W. Li, and W. Shi, "Influence of different blade numbers on unsteady pressure pulsations of internal flow field in mixed-flow pump," *Journal of Drainage and Irrigation Machinery Engineering*, vol. 35, no. 8, pp. 666–673, 2017.

[31] M. Miyabe, H. Maeda, I. Umeki, and Y. Jittani, "Unstable head-flow characteristic generation mechanism of a low specific speed mixed flow pump," *Journal of Thermal Science*, vol. 15, no. 2, pp. 115–120, 2006.

[32] Z. Desheng, S. Weidong, W. Chuan et al., "Influence of impeller and guide vane blade number on pressure fluctuation in mixed-flow pump," *Journal of Drainage and Irrigation Machinery Engineering*, vol. 2, 2012.

[33] T. Lei, Y. Zhiyi, X. Yun, L. Yabin, and C. Shuliang, "Role of blade rotational angle on energy performance and pressure fluctuation of a mixed-flow pump," *Proceedings of the Institution of Mechanical Engineers, Part A: Journal of Power and Energy*, vol. 231, no. 3, pp. 227–238, 2017.

[34] B. Wei and K. Wu, "Investigation into effect of tip clearance on inlet and outlet flow field of diagonal impeller with exit guide volute at near stall condition," *Journal of Engineering Thermophysics*, vol. 21, no. 6, pp. 5–8, 2000.

[35] R. Li, P. Hu, Y. Li et al., "Numerical analysis of effect of blade tip clearance on pressure fluctuation in mixed-flow pump inlet," *Journal of Drainage and Irrigation Machinery Engineering*, vol. 33, no. 7, pp. 560–565, 2015.

[36] Y. Zheng, Y. Chen, X. Mao et al., "Pressure pulsation characteristics and its impact on flow-induced noise in mixed-flow pump," *Transactions of the Chinese Society of Agricultural Engineering*, vol. 31, no. 23, pp. 67–73, 2015.

[37] W. Li, W. Shi, Y. Xu et al., "Effects of guide vane thickness on pressure pulsation of mixed-flow pump in pumped-storage power station," *Journal of Vibroengineering*, vol. 15, no. 3, 2013.

[38] K. Wang, H. Liu, X. Zhou, and W. Wang, "Experimental research on pressure fluctuation and vibration in a mixed flow pump," *Journal of Mechanical Science and Technology*, vol. 30, no. 1, pp. 179–184, 2016.

[39] D. Zindani, A. K. Roy, and K. Kumar, "Design of mixed flow pump impeller blade using mean stream line theory and its analysis," *Scientia Iranica*, vol. 27, no. 1, pp. 350–360, 2020.

[40] S. D. Meyers, B. G. Kelly, and J. J. O'Brien, "An introduction to wavelet analysis in oceanography and meteorology: with application to the dispersion of yanai waves," *Monthly Weather Review*, vol. 121, no. 10, pp. 2858–2866, 1993.

[41] C. Torrence and G. P. Compo, "A practical guide to wavelet analysis," *Bulletin of the American Meteorological Society*, vol. 79, no. 1, pp. 61–78, 1998.